Supporting Information

Atomic Layer Deposited Molybdenum Disulfide on Si Photocathodes for Highly Efficient Photoelectrochemical Water Reduction Reaction

Seungtaeg Oh[‡a], Jun Beom Kim[‡b], Jun Tae Song[a,c], Jihun Oh [*a,c], and Soo-Hyun Kim[*b]

[a]*Graduate School of Energy, Environment, Water, and Sustainability (EEWS), Korea Advanced Institute of Science and Technology (KAIST), 291 Daehak-ro, Yuseong-gu, Daejeon 350-701, Republic of Korea*

[b]*School of Materials Science and Engineering, Yeungnam University, Gyeongsangbuk-do 712-749, Republic of Korea*

[c]*KI Institute for NanoCentury, Korea Advanced Institute of Science and Technology (KAIST), 291 Daehak-ro, Yuseong-gu, Daejeon 350-701, Republic of Korea*

*E-mail: jihun.oh@kaist.ac.kr and soohyun@ynu.ac.kr

[‡]These authors contributed equally.

S1. Images of wafer scale ALD MoS_2

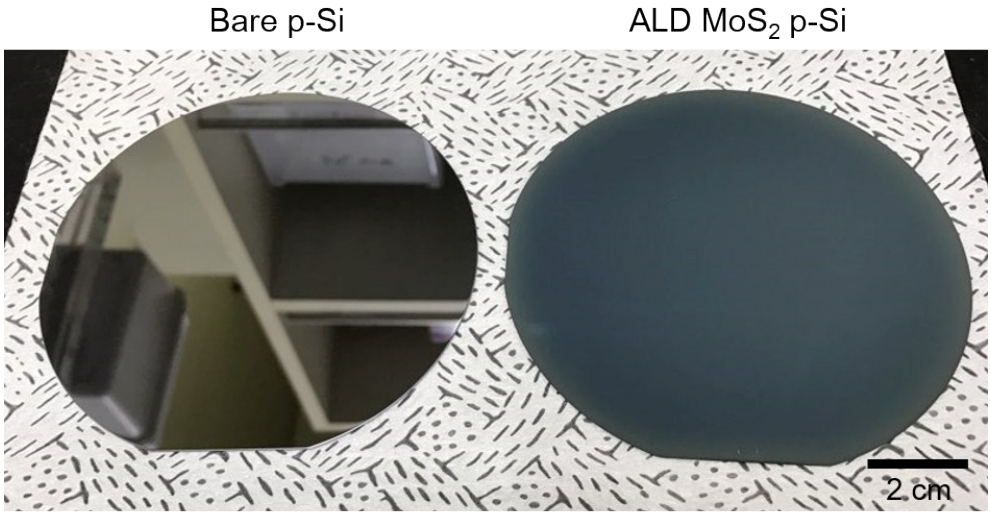

Figure S1. A digital image of a 4 inch p-Si wafer (left) and ALD MoS_2 on 4-inch p-Si wafer with 1180 ALD cycles (right).

S2. SEM images of MoS_2 with various ALD reaction cycles

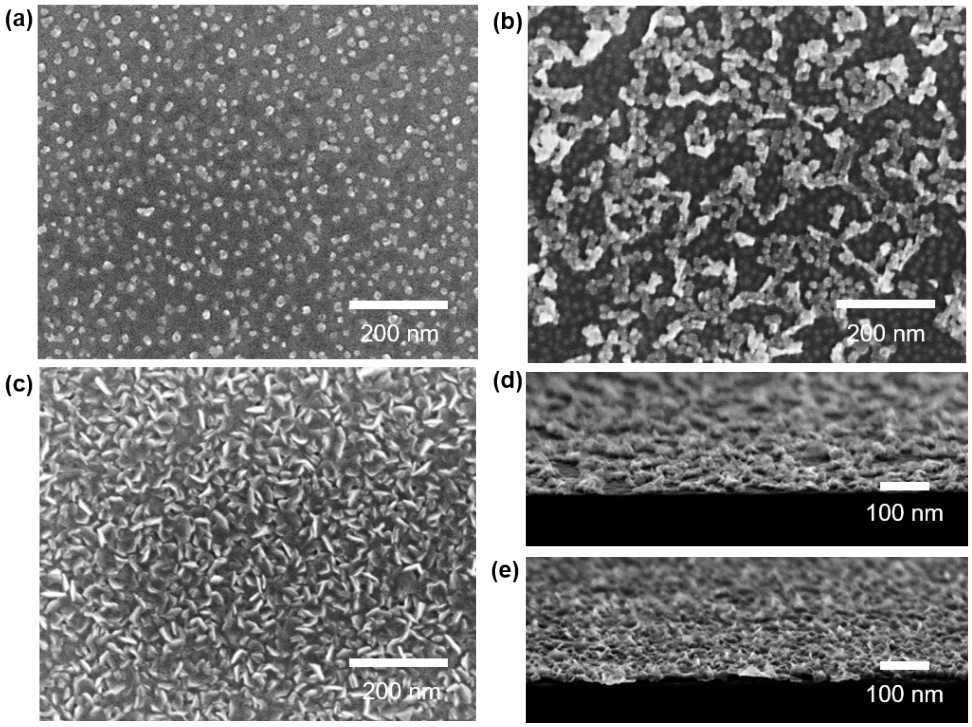

Figure S2. Plan view SEM images of as-grown ALD MoS_2 on p-Si wafers, which were deposited for (a) 60 cycles, (b) 295 cycles, and (c) 1180 cycles. Cross-sectional view SEM image of as-grown ALD MoS_2 film on p-Si wafers, which were deposited for (d) 295 cycles, (e) 1180 cycles.

S3. Growth rates of ALD MoS_2 on Si

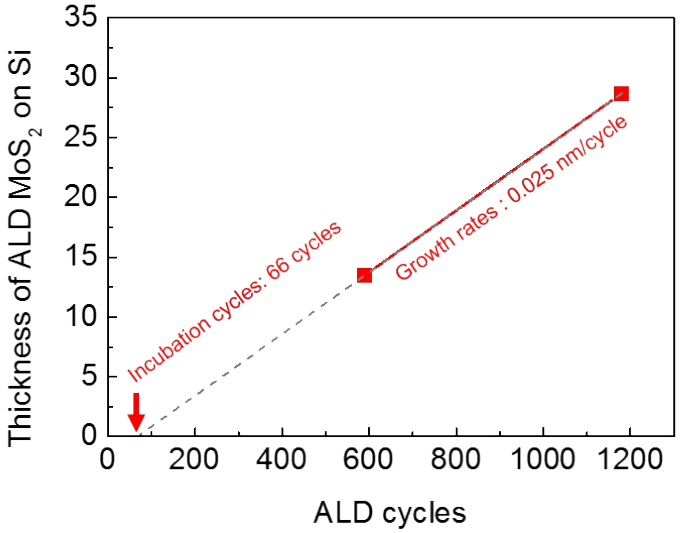

Figure S3. The growth rates of ALD MoS_2 on Si. These data are collected with only continuous ALD MoS_2 film.

S4. XRD and Raman spectra of MoS_2 with various ALD cycles and sulfurization temperatures

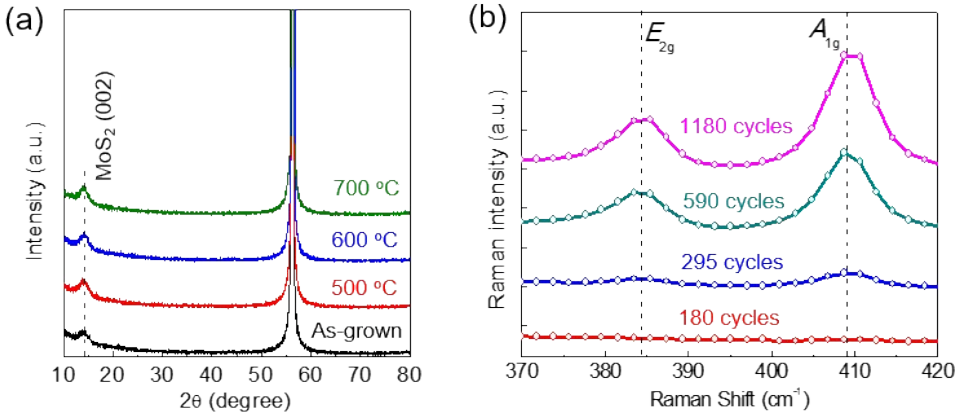

Figure S4. (a) XRD spectra of ALD MoS_2 with various sulfurization temperatures and (b) Raman spectra for sulfurized ALD MoS_2 deposited from 180 to 1180 cycles. Sulfurization temperature is 600 °C.

S5. Electrochemical Impedance Spectroscopy (EIS) of ALD MoS_2 on Si photocathodes

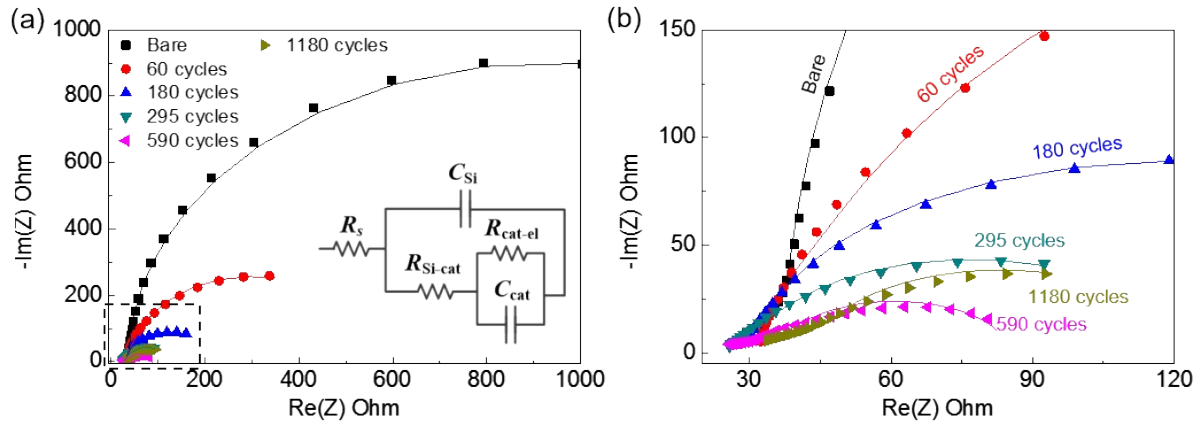

Figure S5. (a) Nyquist impedance plots of sulfurized ALD MoS_2 deposited for reaction cycles from 60 to 1180 cycles. Measurements were carried out at an applied bias of 0 V vs. RHE under 1 sun illumination in 0.5M H_2SO_4. The solid lines correspond to the fitting that uses the equivalent circuit in the inset of (a). (b) The magnified Nyquist plots of the dashed box in (a).

Inset of Fig. S5a shows a simplified equivalent circuit for impedance analysis of ALD MoS_2/p-Si, which was established for photoelectrodes with capacitive co-catalysts, such as MoS_2/Si and Co-Pi/Fe_2O_3.[1, 2] This circuit is composed of 5 elements of resistances and capacitances; a series resistance of Si, MoS_2, and electrolyte, R_s, a capacitance of the Si substrate, C_{Si}, a charge transfer resistance between Si surface and MoS_2, $R_{Si\text{-}cat}$, a resistance between co-catalyst layer and electrolyte, $R_{cat\text{-}el}$, and a capacitance of MoS_2, C_{cat}. Two resistances generated at interface between two different materials are placed in series along for electrons to flow. In addition, since our ALD MoS_2 is thin, two capacitances of Si and MoS_2, C_{Si} and C_{cat}, are placed in parallel in the equivalent circuit. In order to extract resistance values, we performed 3 sets of EIS measurements for each sample. Note that C_{si} in ALD MoS_2/p-Si photocathodes has a range

from 0.1 to 0.4 μF/cm^2 which are consistent to well-known capacitance of p-Si obtained by EIS.[3, 4]

Table S1. Charge transfer resistances of ALD MoS_2 on Si photocathodes.

Photocathode	ALD cycles	R_s (Ω cm^2)	$R_{si\text{-}cat}$ (Ω cm^2)	$R_{cat\text{-}el}$ (Ω cm^2)
Bare p-Si	-	30.5 ±2	-	1622 ±140
Sulfurized ALD MoS_2 Si photocathode	60 cycles	25.5 ±3	143.93 ±20	424.23 ±44
	180 cycles	24.99 ±2	31.19 ±2	144.3 ±15
	295 cycles	27.97 ±3	20.02 ±5	66.37 ±12
	590 cycles	25.57 ±3	14.02 ±2	38.94 ±2
	1180 cycles	36.60 ±8	17.14 ±2	38.56 ±3

Note: R_s is the series resistance of an equivalent circuit; $R_{si\text{-}cat}$ is the resistance at the interface between the catalyst and Si surface; $R_{cat\text{-}el}$ is the resistance at the interface between the electrolyte and catalyst. All resistances are obtained by the average of 3 sets of EIS measurements.

S6. Optical transmittance of MoS_2 on quartz

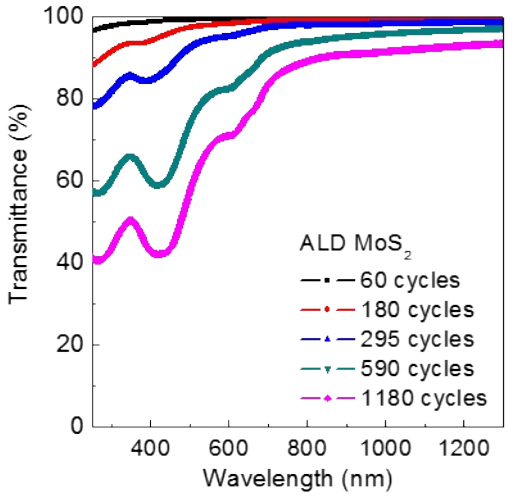

Figure S6. (a) Transmittance of ALD MoS_2 films on quartz that were sulfurized at 600 ^{o}C.

S7. PEC performance comparison of our and previously reported MoS_2 on Si photocathodes

Table S2. PEC performance of previously reported MoS_2 Si photocathodes compared with our studies.

#	Photocathode	V_{on} (V vs RHE)	j_{0V} (mA/cm^2)	j_{sat} (mA/cm^2)	methods	refs
1	MoS_2/p-Si	0.23	21.7	31	ALD	*this work*
2	Pt/p-Si	0.21	17	22.5	Electroless-deposition	*this work*
3	MoS_2/p-Si	0.17	24.6	40	Thermolysis followed by a layer transfer	*5*
4	MoS_2/TiO_2/p-Si NW	0.25	15	25	Thermolysis of spin-coated precursors	*6*
5	1T-MoS_2/p-Si	0.25	17.5	26.7	CVD	*7*
6	a-$CoMoS_x$/p-Si	0.25	17.5	20	Photo-assisted electrodeposition	*2*
7	MoS_2/Mo/n^+p-Si	0.32	17	17.5	Direct sulfurization of Mo layer	*8*
8	a-MoS_x/Ti/n^+p-Si	0.33	16	16	Electrodeposition	*9*

Note: V_{on} is the onset potential that is required for producing 1 mA/cm^2 of current density; j_{0V} is the photocurrent density measured at an applied bias 0 V vs RHE; j_{sat} is the saturation photocurrent density of photocathode; 1T-MoS_2 is the metallic crystalline MoS_2; n^+p is the phosphorus doped Si emitter layer; Si NW is silicon nanowire; CVD is chemical vapor deposition.

S8. Pt/p-Si Si photocathode

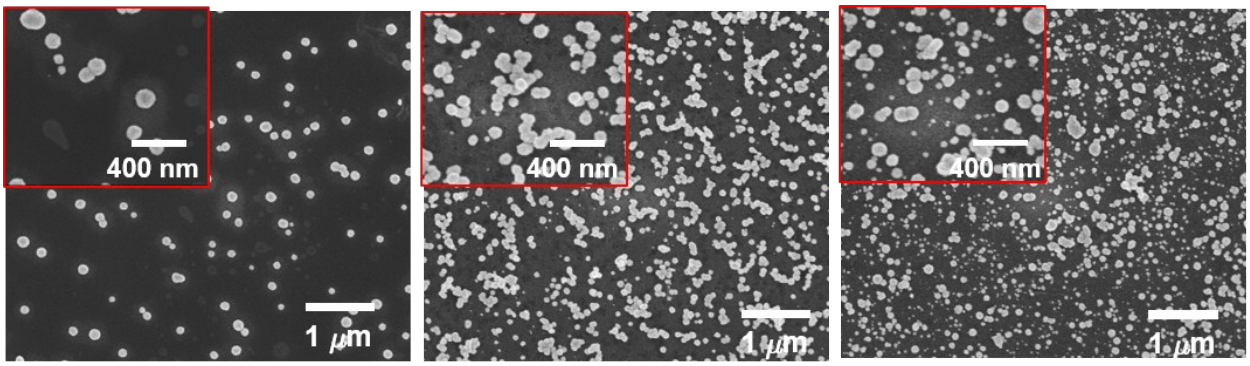

Figure S7. Plan view SEM images of p-Si with Pt nanoparticles deposited for (a) 5, (b) 9, and (c) 12 minutes. Each inset image indicates high resolution plan view SEM images of Pt/p-Si.

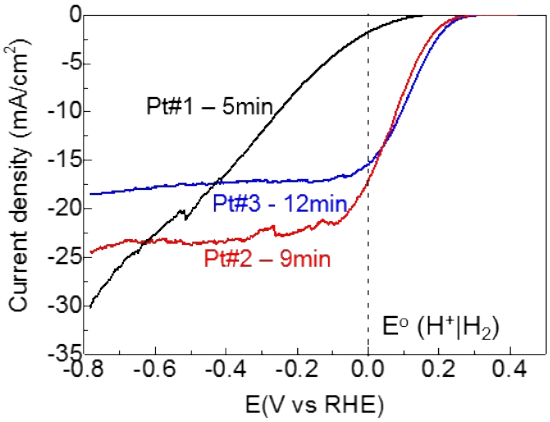

Figure S8. PEC *j-V* curves of p-Si with Pt nanoparticles deposited for 5 (black solid line), 9 (red solid line), and 12 (blue solid line) minutes in 0.5 M H_2SO_4 under simulated 1 sun illumination.

REFERENCES

1. B. Klahr, S. Gimenez, F. Fabregat-Santiago, J. Bisquert and T. W. Hamann, *J. Am. Chem. Soc.*, 2012, **134**, 16693-16700.
2. Y. Chen, P. D. Tran, P. Boix, Y. Ren, S. Y. Chiam, Z. Li, K. Fu, L. H. Wong and J. Barber, *ACS nano*, 2015, **9**, 3829-3836.
3. M. Chemla, J.-F. Dufrêche, I. Darolles, F. Rouelle, D. Devilliers, S. Petitdidier and D. Levy, *Electrochimica acta*, 2005, **51**, 665-676.
4. M. Hecini, A. Khelifa, B. Palahouane, S. Aoudj and H. Hamitouche, *Research on Chemical Intermediates*, 2015, **41**, 327-341.
5. K. C. Kwon, S. Choi, K. Hong, C. W. Moon, Y.-S. Shim, D. H. Kim, T. Kim, W. Sohn, J.-M. Jeon and C.-H. Lee, *Energy Envrion. Sci.*, 2016.
6. L. Zhang, C. Liu, A. B. Wong, J. Resasco and P. Yang, *Nano Research*, 2015, **8**, 281-287.
7. Q. Ding, F. Meng, C. R. English, M. Cabán-Acevedo, M. J. Shearer, D. Liang, A. S. Daniel, R. J. Hamers and S. Jin, *J. Am. Chem. Soc.*, 2014, **136**, 8504-8507.
8. J. D. Benck, S. C. Lee, K. D. Fong, J. Kibsgaard, R. Sinclair and T. F. Jaramillo, *Advanced Energy Materials*, 2014, **4**.
9. B. Seger, A. B. Laursen, P. C. Vesborg, T. Pedersen, O. Hansen, S. Dahl and I. Chorkendorff, *Angewandte Chemie International Edition*, 2012, **51**, 9128-9131.